Extended Data Fig.1: DFCP1 is an ancient protein.

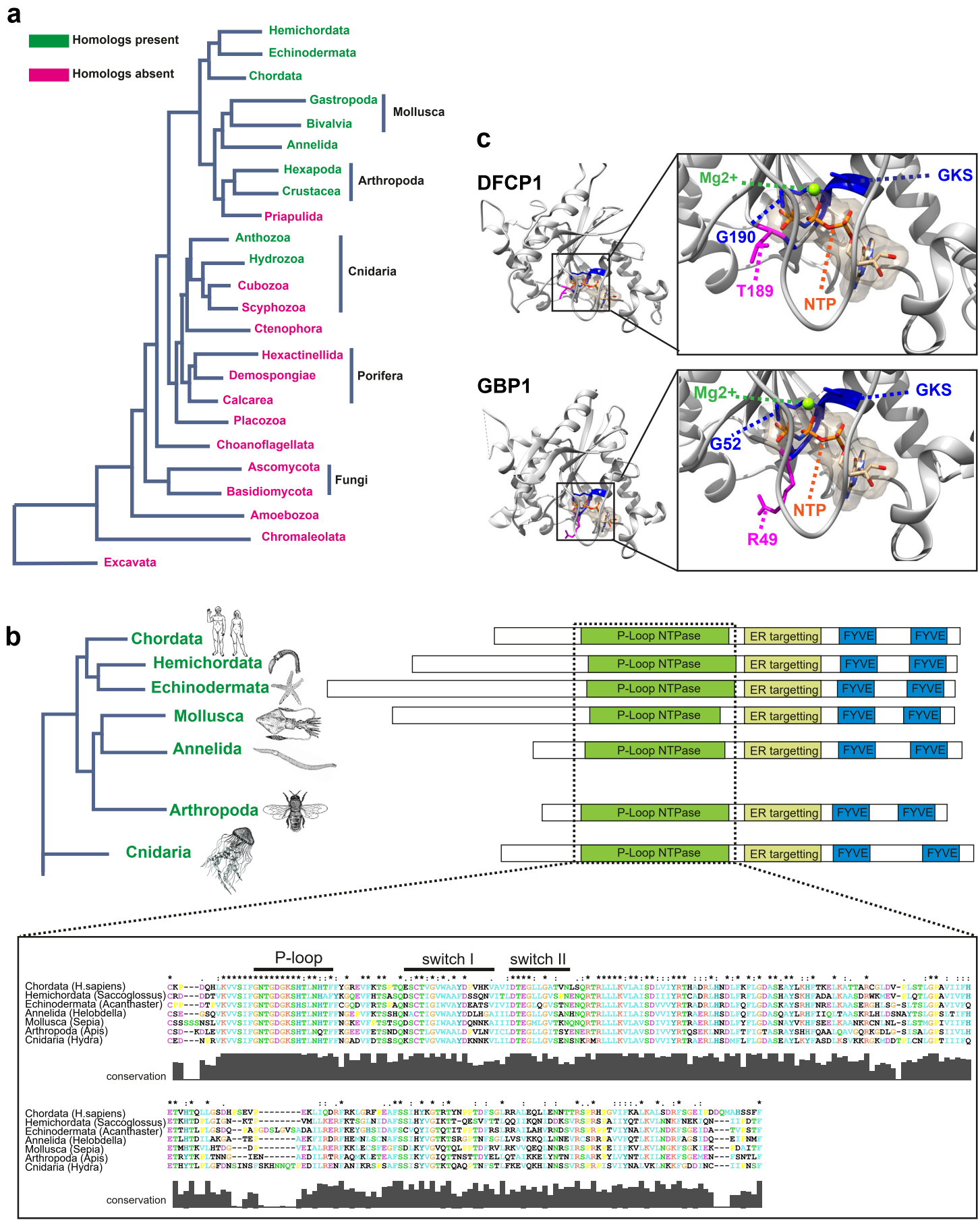

Extended Data Fig.1: DFCP1 is an ancient protein.

(a) DFCP1 is conserved in the animal kingdom. Homologs of DFCP1 first occur in the cnidarian phylum and is present in nearly all metazoan phyla, indicating that it was first invented more than 0.5 billion years ago.

(b) The domain structure of DFCP1 is highly conserved throughout the metazoan tree of life. The DFCP1 domain architecture has remained largely unchanged from the first occurrence in the cnidarians. All homologs have a highly conserved ATP binding domain, an ER-binding domain and two FYVE domains.

(c) Phyre2-generated homology model of DFCP1, based on the structure of GBP1. Candidates for amino acids required for nucleotide binding (GKS, residues 192-194) are indicated in blue, and amino acids at the same position as the catalytic arginine of GBP1 (T189, G190) and KRAS (G12, G13) are indicated in magenta.

Extended Data Fig.2: DFCP1 binds and hydrolyses ATP.

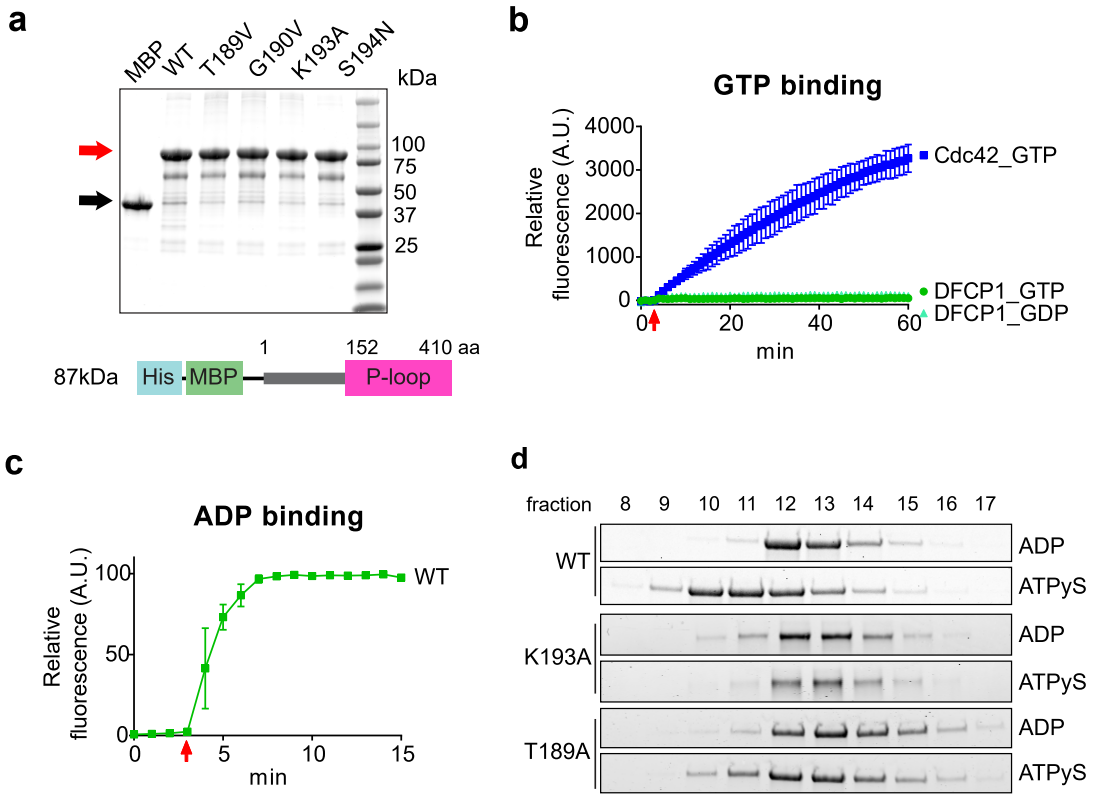

Extended Data Fig.2: DFCP1 binds and hydrolyses ATP.

(a) Coomassie gel from purified DFCP1 N-terminus as used in Fig.1d-h and Extended Data Fig.2b-d. Red arrow indicates MBP-DFCP1 for a calculated mass of 87kDa, black arrow indicates MBP (43 kDa). Schematic overview of the His- and MBP-tagged N-terminus including P-loop of DFCP1 (DFCP1 K193A or DFCP1 T189A) used for nucleotide binding measurements.

(b) DFCP1 does not bind guanosine nucleotides. Recombinant DFCP1 WT was incubated in the presence of mantGTP (n=4) or mantGDP (n=3) (arrow). Nucleotide binding was measured by incorporation of fluorescent mantGDP/GTP. Purified Cdc42 was used as a positive control for GTP binding (n=2). Curves are normalized to MBP (DFCP1) or GST (Cdc42) background fluorescence. Bars: mean ± SD.

(c) DFCP1 binds to adenosine nucleotides. DFCP1 WT was incubated with mantADP (arrow), and nucleotide binding was measured by the incorporation of fluorescent mantATP/ADP. Curve is normalized to MBP background fluorescence. Bars: mean ± SD, 3 experiments.

(d) Coomassie gel showing individual 1 ml fractions of the size exclusion chromatography shown in Fig.1h.

Extended Data Fig.3: Characterization of DFCP1 KO- and kd- rescue systems.

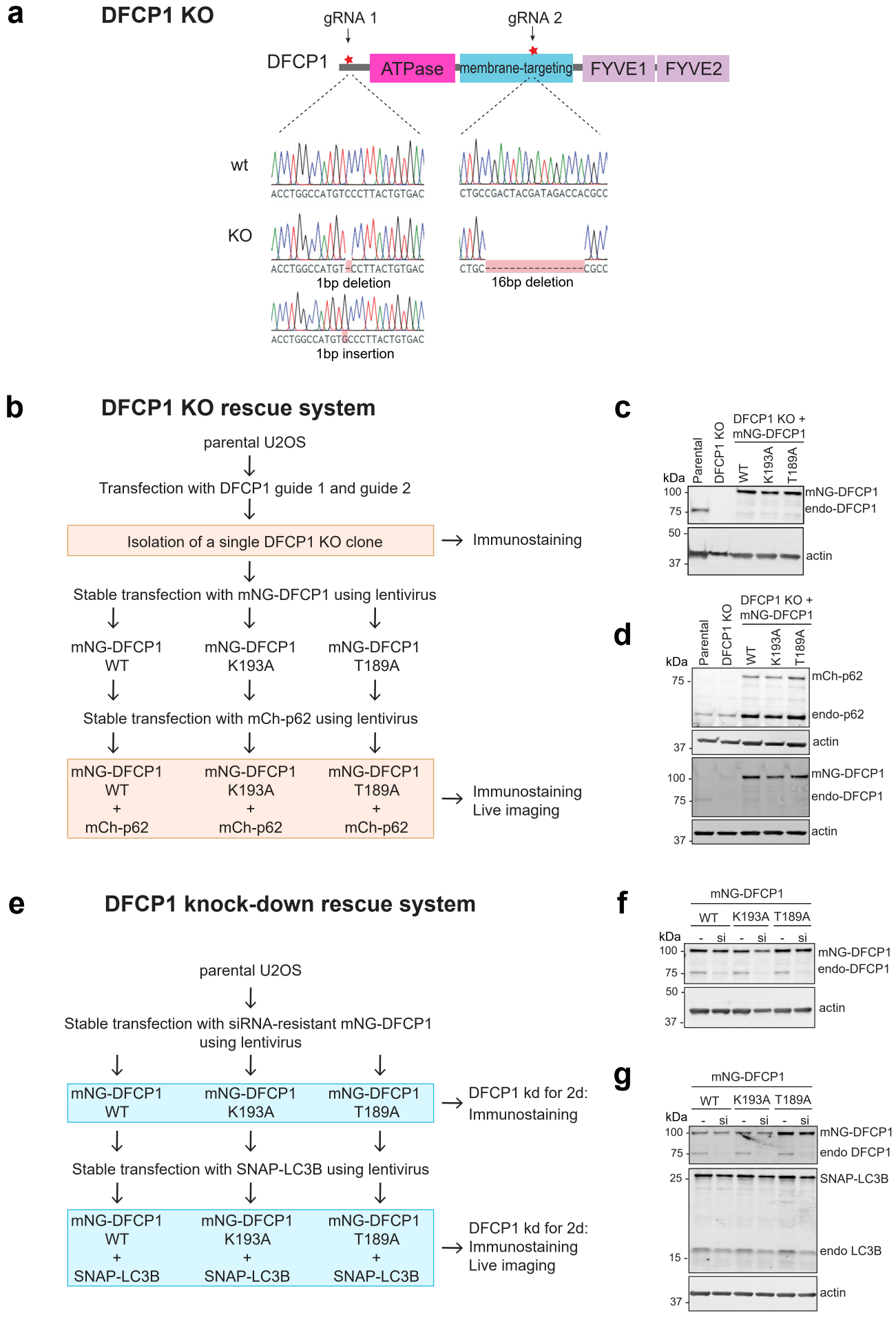

Extended Data Fig.3: Characterization of DFCP1 KO- and knockdown-rescue systems.

(a) Generation and characterization of CRISPR/Cas9-mediated DFCP1 KO in U2OS cells. Shown are the localization of guide RNAs targeting DFCP1 and the sequences of a single clone which was isolated and validated by Sanger sequencing. This clone has been utilized for all further experiments.

(b) Schematic drawing of the generation of the DFCP1 KO rescue system. DFCP1 KO cells were stably transduced with a low titer of mNG-DFCP1 WT, K193A or T189A. These lines were further transduced with mCh-p62, and cells have been imaged live in EBSS for omegasome quantification (Fig.2, Extended Data Fig.4a-c).

(c) Western blotting was used to measure protein levels of endogenous DFCP1 and mNG-DFCP1 using anti-DFCP1 antibody. Actin was used as loading control.

(d) Western blotting was used to measure protein levels of endogenous and exogenous expressed DFCP1 and p62 using anti-DFCP1 and anti-p62 antibodies. Actin was used as loading control.

(e) Schematic drawing of the generation of the DFCP1 knockdown-rescue system for confocal imaging. U2OS cells were stably transduced with a low titer of siRNA-resistant mNG-DFCP1 WT, K193A or T189A. The resulting stable cell lines were then transfected with siRNA against DFCP1 for 2 d and treated as mentioned. Alternatively, cells were transduced with lentiviral vectors expressing SNAP-LC3B and cells were imaged live in EBSS for omegasome quantification (Extended Data Fig4.d-i).

(f) Western blotting was used to validate knockdown of DFCP1 using anti-DFCP1 antibody. Actin was used as loading control.

(g) Western blotting was used to measure protein levels of DFCP1 and LC3B, actin was used as loading control.

Extended Data Fig.4: DFCP1 mutants are delayed in omegasome constriction.

DFCP1 KO rescue system

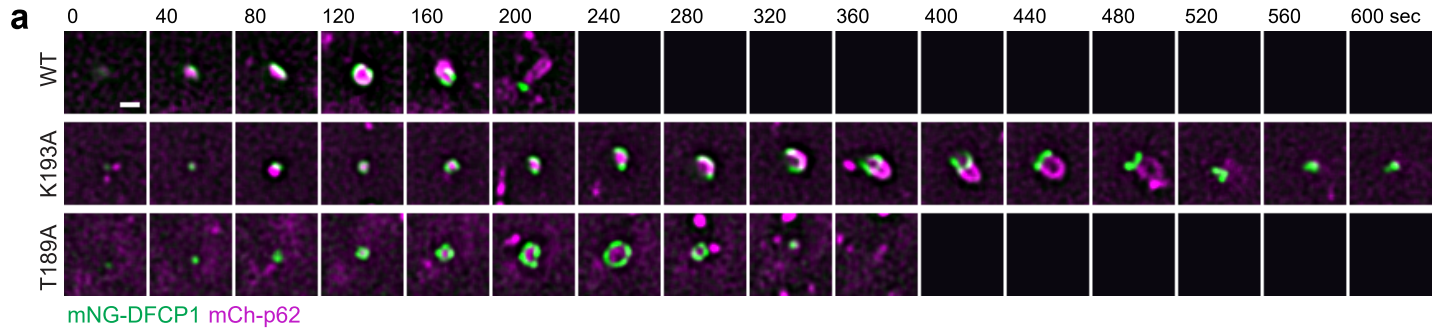

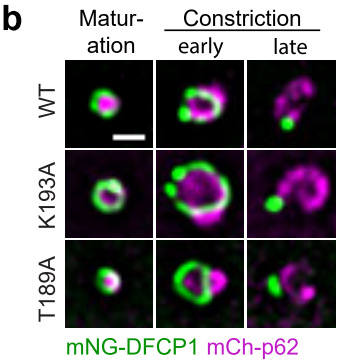

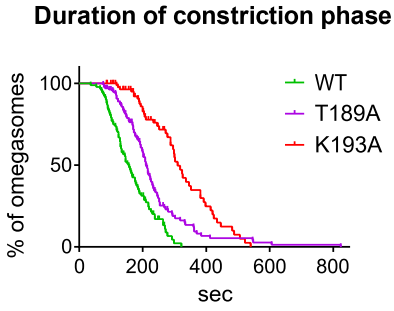

DFCP1 knock-down rescue system

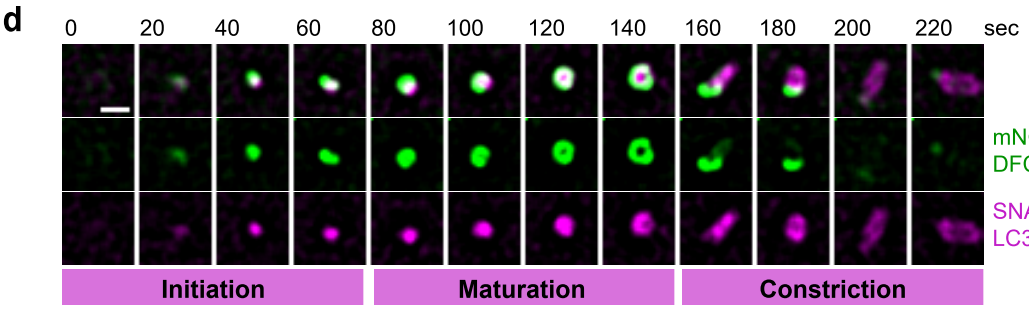

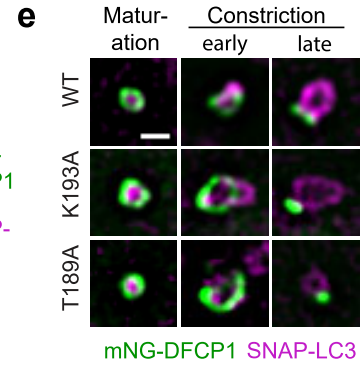

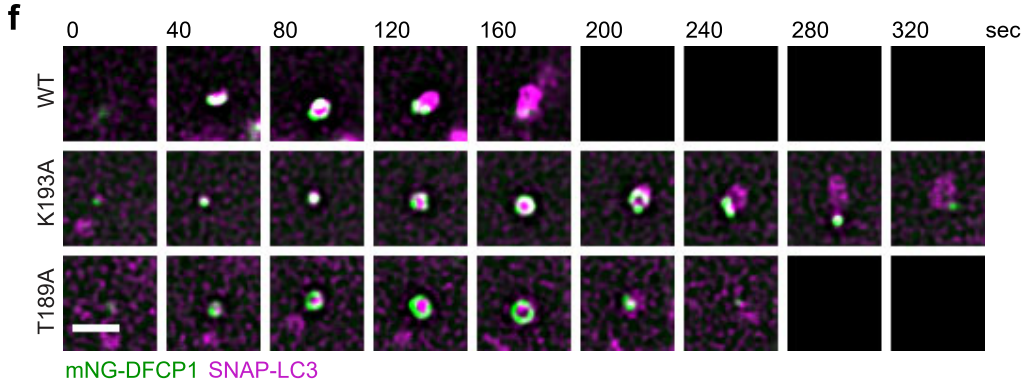

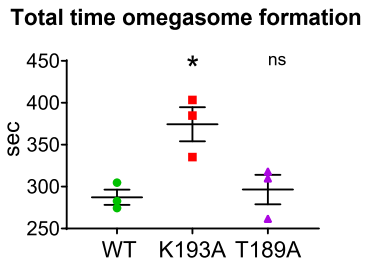

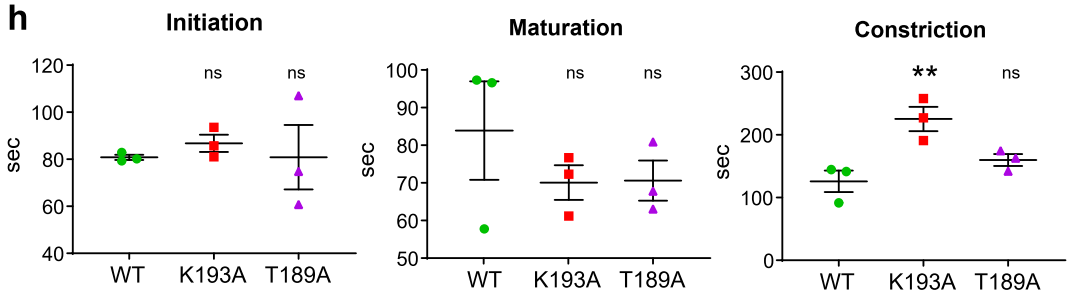

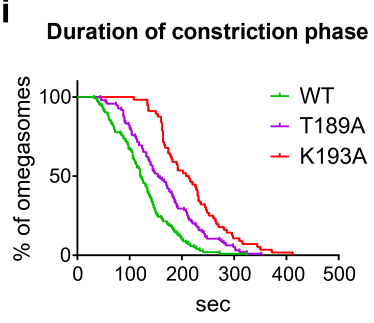

Extended Data Fig.4: DFCP1 mutants are delayed in omegasome constriction.

(a) U2OS DFCP1 KO lines stably expressing mNG-DFCP1 WT or -mutant and mCh-p62. Cells were starved with EBSS and imaged live to capture omegasome formation. Shown are representative stills of omegasomes analyzed in Fig.2b, c. Scale bar 0.5 µm.

(b) Examples of omegasomes from cells expressing DFCP1 WT or mutant DFCP1. U2OS DFCP1 KO lines stably expressing mNG-DFCP1 WT and mCh-p62 were starved in EBSS and imaged live to capture omegasome formation. The first image shows the ring phase, with p62 localizing in the middle. The second image shows the time point which was used as the onset of the constriction phase. A p62-positive autophagosome with a remaining DFCP1 dot is shown in the third image. Scale bar 0.5 µm. Representative image of > 20 events.

(c) Duration of the constriction phase of single omegasomes plotted over time. The quantification is derived from the same raw data as in Fig.2b-d.

(d) U2OS DFCP1 knockdown/rescue lines stably expressing mNG-DFCP1 WT and SNAP-LC3B were depleted by endogenous DFCP1 for 2 d, starved with EBSS and imaged live to capture omegasome formation. Omegasome formation was divided into three phases as indicated. Shown are representative stills of omegasomes analyzed in (g) and (h). Scale bar 0.5 µm.

(e) Examples of omegasomes from DFCP1 knockdown rescue lines expressing mNG-DFCP1 WT or -mutant and SNAP-LC3B. The first image shows the ring phase, with SNAP-LC3B localizing in the middle. The second image shows the time point which was defined as the onset of the constriction phase. A LC3B-positive autophagosome with a remaining DFCP1 dot is shown in the third image. Scale bar 0.5 µm. Representative image of > 40 events.

(f) U2OS DFCP1 knock-down rescue lines stably expressing mNG-DFCP1 WT or -mutant and SNAP-LC3B were depleted by endogenous DFCP1 for 2 d, starved with EBSS and imaged live to capture omegasome formation. Scale bar 0.5 µm.

(g) Total time of an omegasome life cycle, with a DFCP1 punctum as beginning and -end points. Each plotted point represents the mean value of one experiment. Bars: mean ± SEM, 3 experiments. Statistics: One-way ANOVA followed by Dunnett's multiple comparisons test, comparing against WT. Analyzed omegasomes per genotype: WT=93, K193A=45, T189A=89.

(h) Duration of the individual phases of omegasome formation. Each plotted point represents the mean value of one experiment. The quantification is derived from the same raw data as (f) and (g). Bars: mean ± SEM, 3 experiments. Statistics: One-way Anova followed by Dunnett's multiple comparisons test, comparing against WT. Analyzed omegasomes per genotype and phase: Initiation: WT=77, K193A= 48, T189A=76; Maturation: WT=87, K193A=56, T189A=83; Constriction: WT=103, K193A=56, T189A=92.

(i) Duration of the constriction phase of single omegasomes plotted over time. The quantification is derived from the same raw data as in (g) and (h).

Extended Data Fig.5: Omegasome initiation is not affected in DFCP1 ATPase mutants.

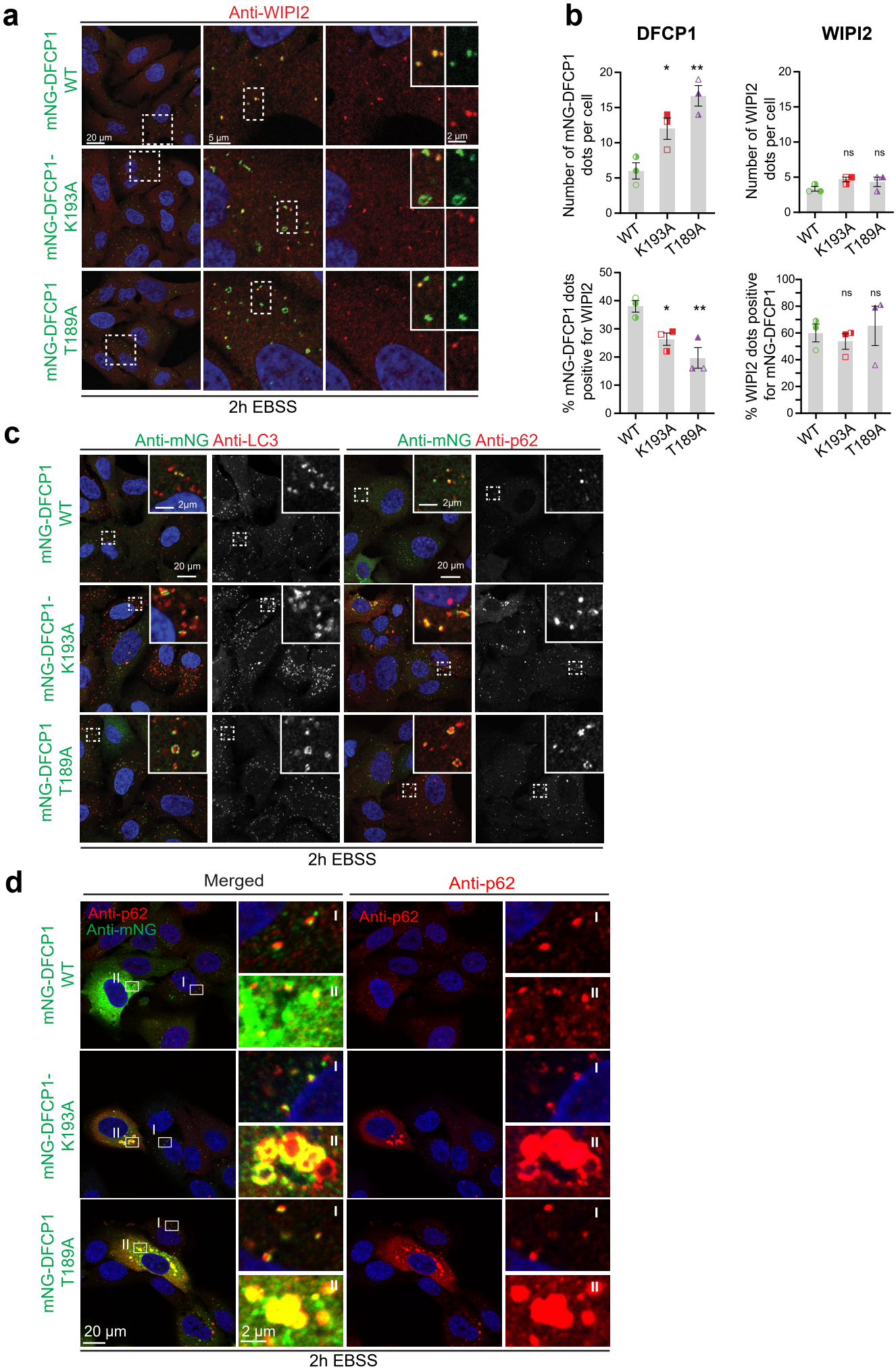

Extended Data Fig.5: Omegasome initiation is not affected in DFCP1 ATPase mutants.
Fixed imaging of U2OS DFCP1 knock-down rescue lines stably expressing mNG-DFCP1 WT, K193A or T189A as indicated:

(a) Confocal images showing the localization and abundance of WIPI2 puncta in DFCP1 mutant cells. U2OS cells stably expressing siRNA resistant mNG-DFCP1 WT, K193A or T189A, were depleted of endogenous DFCP1 by siRNA transfection for 2 d in complete medium before starvation for 2 h in EBSS. The cells were fixed, stained with anti-WIPI2 antibody, and analyzed by confocal microscopy. Insets show that some of the DFCP1-positive omegasomes co-localize with WIPI2. Representative image for (b). Scale bar 20 µm, insets 5 µm and 2 µm.

(b) Graphs represent quantifications of (a) of the amount of mNG-DFCP1 dots and WIPI2 dots per cell and the co-occurrence between DFCP1 and WIPI2 dots, from images like described above. Error bars denote mean ± SEM, 3 experiments. Each plotted point represents the mean value of one experiment, and independent experiments are indicated by different colored or transparent objects. Ordinary one-way ANOVA, Dunnett's post hoc test: * $p < 0.05$; ** $p < 0.01$; ns: not significant. Analyzed cells per condition: WT= 268, K193A= 273, T189A= 227.

(c) Representative images of the quantifications shown in Fig.3c. Confocal images showing the localization of DFCP1, DFCP1 mutants, LC3B and p62 in DFCP1 KD rescue cell lines. U2OS cells stably expressing siRNA resistant mNG-DFCP1-WT, K193A, or T189A were depleted of endogenous DFCP1 by siRNA transfection for 2 d in complete medium before starvation for 2 h in EBSS. Cells were fixed, stained with anti-mNG and either anti-LC3B or anti-p62 antibodies and analyzed by confocal microscopy. Both LC3B and p62 are found in close association with DFCP1 positive omegasomes. Note that the localization of p62 is more restricted to omegasomes than LC3B. Quantifications in Fig3c, d. Scale bar 20 µm, inset 2 µm.

(d) U2OS cells stably expressing DFCP1 WT, K193A, T189A were depleted of endogenous DFCP1 by siRNA, treated with EBSS for 2 h, fixed and stained with anti-mNG and anti-p62 antibodies and analyzed by confocal microscopy. p62 colocalizes with DFCP1 in high and low expressing DFCP1 cells under all conditions. Notably, strong overexpression of the ATPase defective DFCP1 T189A allele causes hyper-accumulation of p62. Such cells, which appeared with low frequency in the stable cell lines, were not included in the high content-based image quantifications. Representative of >5 images per condition.

Extended Data Fig.6: While bulk autophagy is not affected, the levels of p62 are elevated in DFCP1 ATPase mutants.

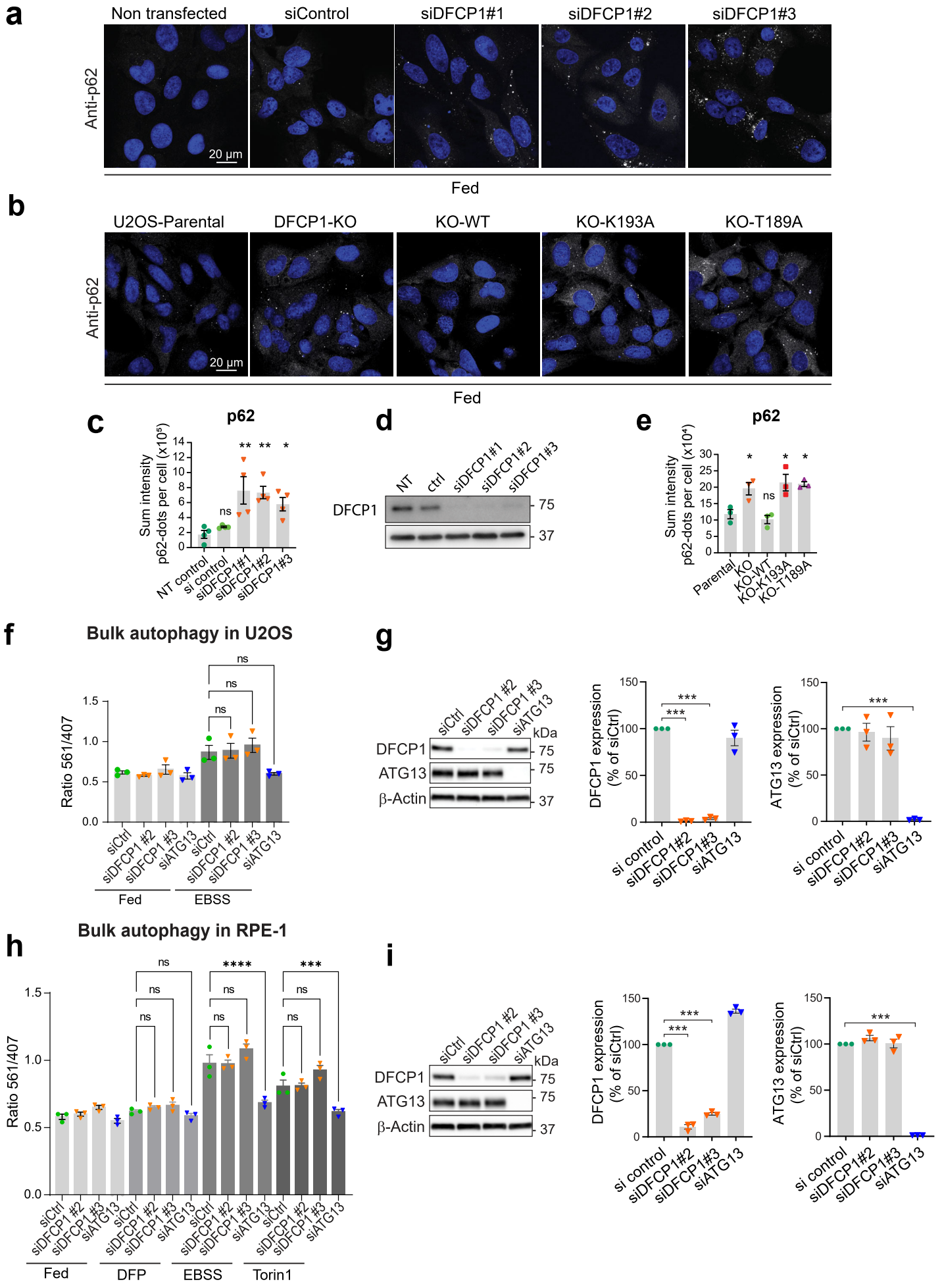

Extended Data Fig.6: While bulk autophagy is not affected, the levels of p62 are elevated in DFCP1 ATPase mutants.

(a) U2OS cells were depleted of endogenous DFCP1 by siRNA transfection for 2 d in complete medium, fixed, stained with anti-p62 antibody and Hoechst33342, and analyzed by confocal microscopy. Scale bar 20 µm.

(b) U2OS parental cells and DFCP1 KO rescue cells cultured in complete medium, were fixed and stained with anti-p62 antibody and Hoechst33342 and analyzed by confocal microscopy. Scale bar 20 µm.

(c) Quantifications of (a). Graphs represent quantification of the sum intensity of p62 dots per cell. Error bars denote mean ±SEM, 4 experiments. Each plotted point represents the mean value of one experiment. Ordinary one-way ANOVA, Dunnett's post hoc test: * $p < 0.05$; ** $p < 0.01$; ns: not significant. Total cells analyzed per condition: NT (non-transfected): 575, siCtr= 507, si#1= 464, si#2= 504, si#3= 507.

(d) Western blotting was used to validate knockdown of DFCP1 in (a) using anti-DFCP1 antibody. Actin was used as loading control. Representative blot from n=4 experiments.

(e) Quantification of the experiment shown in (b). Graphs represent quantification of the sum intensity of p62 dots per cell. Error bars denote mean ± SEM from n=3 independent experiments. Each plotted point represents the mean value of one experiment. Ordinary one-way ANOVA, Dunnett's post hoc test: * $p < 0.05$; ns: not significant. Cells analyzed per condition: parental: 788; KO:703; WT: 732, K193A: 779, T189A: 766.

(f) U2OS cells induced to express free cytoplasmic mKeima were transfected with control-, DFCP1- or ATG13 siRNA for 2 d. Cells were either grown for 16 h in complete medium or starved in EBSS. Cells were harvested and subjected to Flow Cytometry to determine the ratio of lysosome-localized mKeima to free, cytoplasmic mKeima. Bars: ±SEM, 3 experiments. Statistics: One-way Anova followed by Dunnett's multiple comparisons test.

(g) Knockdown validation for (f) with Western Blot and quantification of DFCP1- and ATG13 bands using Actin as a loading control. Values were normalized to control siRNA. Bars: ±SEM, 3 experiments. Statistics: Welch's test, comparing against siCtrl.

(h) RPE-1 cells induced to express LDHB-mKeima were transfected with control-, DFCP1- or ATG13 siRNA for 2 d. Cells were cultured for 16 h either in complete medium, in 0.5 mM DFP, were starved in EBSS, or treated with 50 nM Torin1. Cells were harvested and subjected to Flow Cytometry to determine the ratio of lysosome-localized LDHB-mKeima to free, cytoplasmic LDHB-mKeima. Bars: ± SEM, 3 experiments. Statistics: One-way Anova followed by Dunnett's multiple comparisons test.

(i) Knockdown validation for (h) with Western Blot and quantification of DFCP1- and ATG13 bands using Actin as a loading control. Values were normalized to control siRNA. Bars: ±SEM, 3 experiments. Statistics: One sample t-test, comparing against a theoretical mean of 100.

Extended Data Fig.7: DFCP1 ATPase regulates selective types of autophagy.

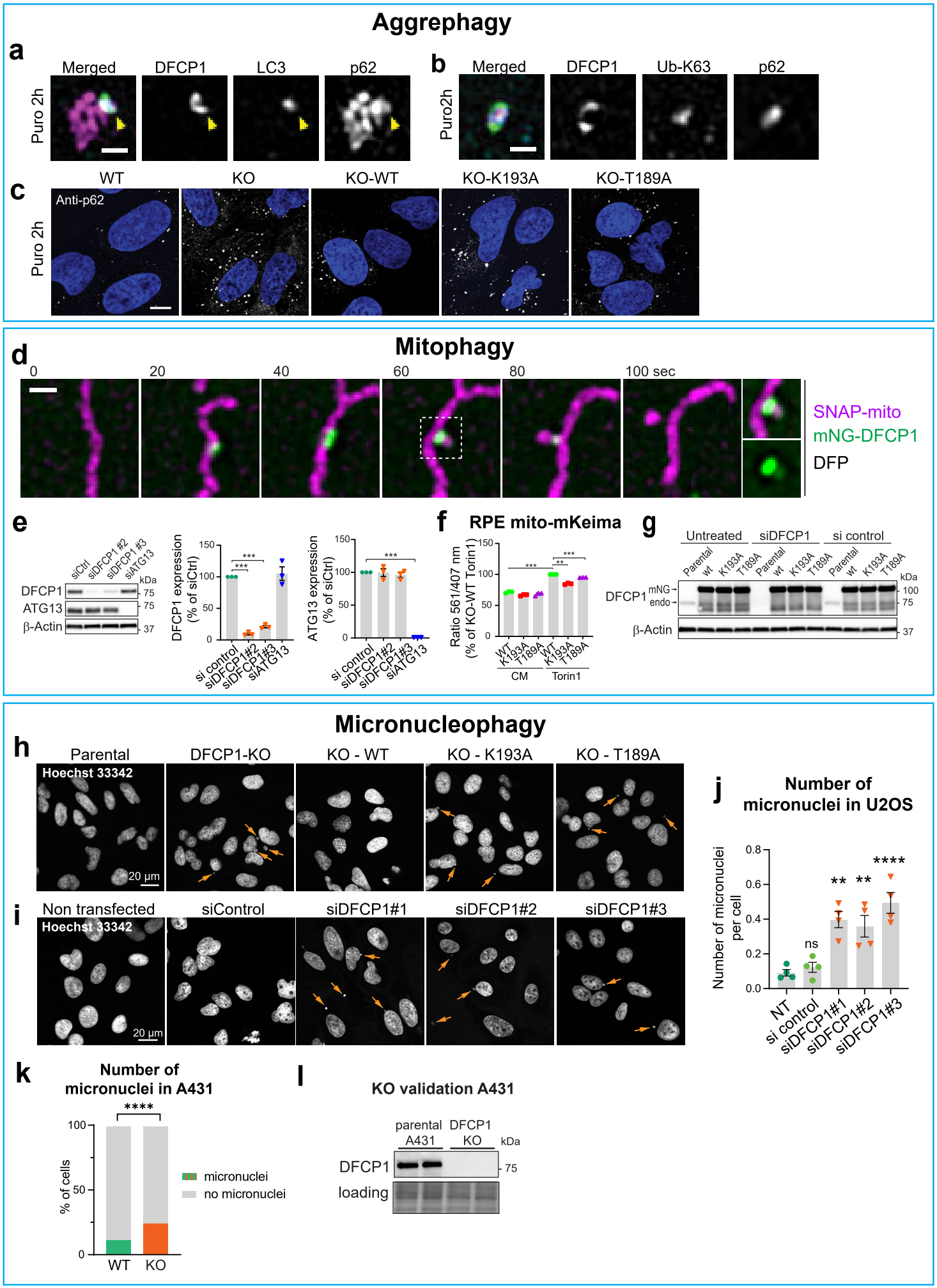

Extended Data Fig.7 DFCP1 ATPase regulates selective types of autophagy.

(a) U2OS stably expressing mNG-DFCP1 WT were treated with 2.5 µg/ml Puromycin for 2 h, fixed, stained with anti-p62 and anti-LC3B antibodies, and analyzed by super-resolution microscopy. Arrowheads denote omegasome rings with a lumen. Scale bar: 0.5 µm.

(b) Cells treated as in (a) were stained with anti-p62 and anti-ubiquitin K63 antibodies and analyzed by super-resolution microscopy. Scale bar: 0.5 µm.

(c) Parental U2OS, DFCP1 KO and KO rescue lines stably expressing mNG-DFCP1 WT, K193A or T189A were treated with 2.5 µg/ml Puromycin for 2 h, fixed, stained with anti-p62 antibody, and analyzed by confocal microscopy. Quantifications in Fig.4c. Scale bar: 10 µm.

(d) Example of a mitophagy event. U2OS cells stably expressing mNG-DFCP1 WT and SNAP-mito were treated for 18 h with 0.5 mM DFP and imaged live. Note the lumen of the omegasome ring, through which a part of the mitochondria is threaded. Scale bar: 1 µm. Representative movie for > 10 events.

(e) Knockdown validation for Fig.4e with Western Blot. Quantification of DFCP1- and ATG13 bands using Actin as a loading control. Values were normalized to control siRNA. Bars: ±SEM, 3 experiments. Statistics: One sample t-test, comparing against a theoretical mean of 100.

(f) RPE-1 cells stably expressing mitochondrial mKeima probe and siRNA resistant mNG-DFCP1-WT, K193A, or T189A were depleted of endogenous DFCP1 by siRNA transfection for 2 d in complete medium (CM) before treatment with 50 nM Torin1 to induce mitophagy. Cells were harvested and analyzed by Flow Cytometry to determine the ratio of lysosome-localized mito-mKeima to free, cytoplasmic mito-mKeima. Values were normalized to the parental control. Bars: ± SEM, 3 experiments. Statistics: One-sample t-test, comparing against a theoretical mean of 100.

(g) Knockdown validation for (f) with Western Blot.

(h) U2OS parental cells, DFCP1-KO and KO rescue lines stably expressing mNG-DFCP1 WT, K193A or T189A were grown in complete medium, fixed, stained with Hoechst33342, and analyzed by confocal microscopy. Arrows point to micronuclei. Quantifications in Fig.4h. Scale bar: 20 µm. Same images as in Extended Data Fig.6b, which show p62 accumulation upon DFCP1 KO. Quantification of MN in Fig.4h.

(i) Parental U2OS cells were depleted of endogenous DFCP1 by siRNA transfection for 2 d in complete medium, fixed, stained with Hoechst33342, and analyzed by confocal microscopy. Arrows point to micronuclei. Same images as in Extended Data Fig.6a, which show p62 accumulation upon DFCP1 depletion.

(j) Quantification of number of micronuclei per cell from (i). Error bars denote mean ± SEM, 4 experiments. Each plotted point represents the mean value of one experiment. One-way ANOVA, Dunnett's post hoc test: ** $p < 0.01$; **** $p < 0.0001$; ns: not significant. Cells analyzed per condition: NT (non-transfected): 575, siCtr: 507, si#1: 464, si#2: 504, si#3: 507. Re-analysis of the images from dataset Extended Data Fig.6a for scoring of micronuclei.

(k) Quantification of number of micronuclei in parental A431 and DFCP1 KO cells. Cells have been grown in complete medium, fixed and stained with DAPI, and analysed by widefield microscopy. Two-sided Fisher's exact test $p < 0.0001$. Data pooled from n=2 experiments. Cells analysed in total: WT=1230, KO=1148.

Extended Data Fig.8: DFCP1 interacts with ubiquitin.

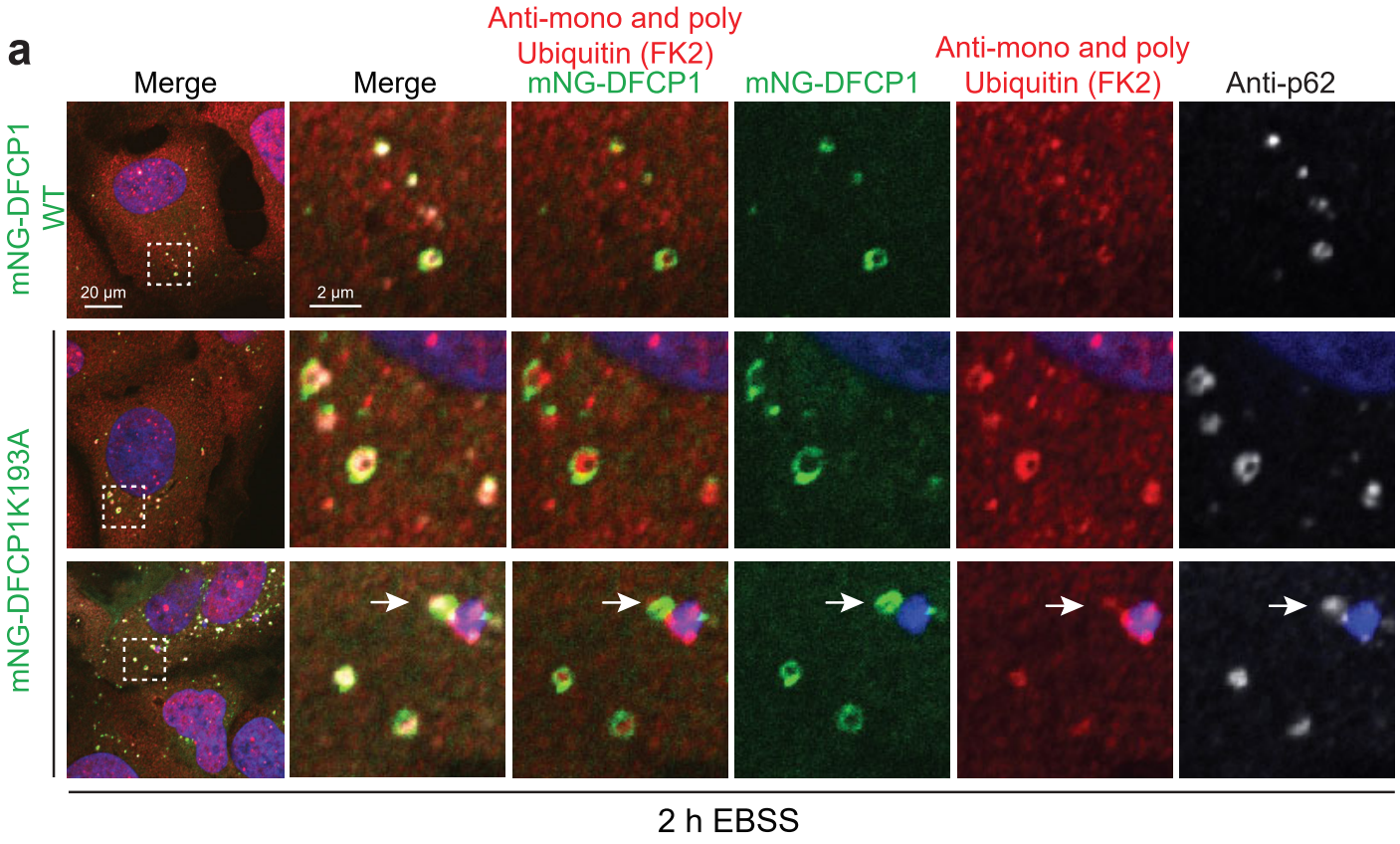

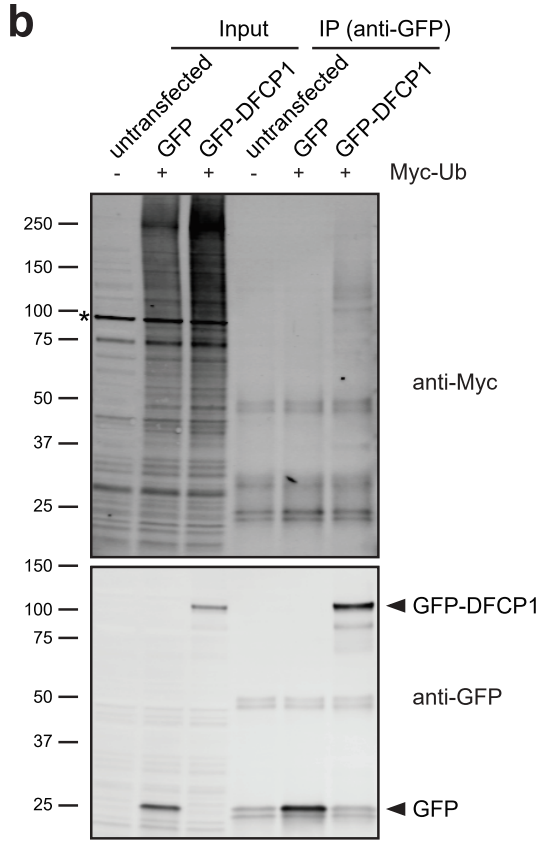

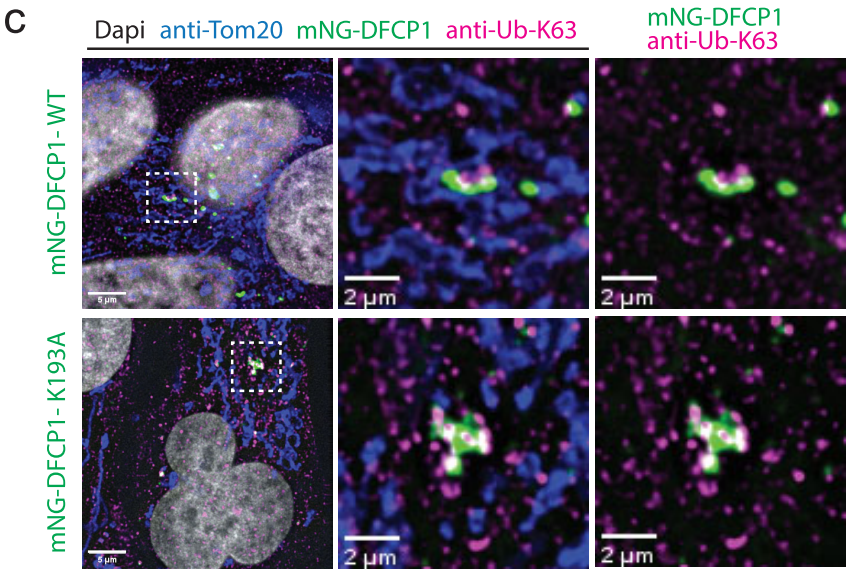

Extended Data Fig.8: DFCP1 interacts with ubiquitin.

(a) U2OS DFCP1 KO lines stably expressing DFCP1 WT or K193A were depleted of endogenous DFCP1 by siRNA, treated with EBSS for 2 h, fixed and stained with anti-mNG, anti-Ubiquitin and anti-p62 antibodies and analyzed by confocal microscopy. Arrows denote an omegasome localizing to a micronucleus. Scale bar 20 µm, insets 2 µm.

(b) Co-IP of transfected HeLa cells. Western blot is representative for 3 independent experiments. Asterisk (*) indicates an unspecific band.

(c) U2OS DFCP1 knockdown/rescue lines stably expressing mNG-DFCP1 WT or K193A were treated with DFP 0.5 mM for 18h to induce mitophagy, fixed, stained with anti-Tom20, anti-mNG and anti-Ub-K63 antibodies, and analyzed by widefield microscopy. Scale bar 5 µm, insets 1 µm.

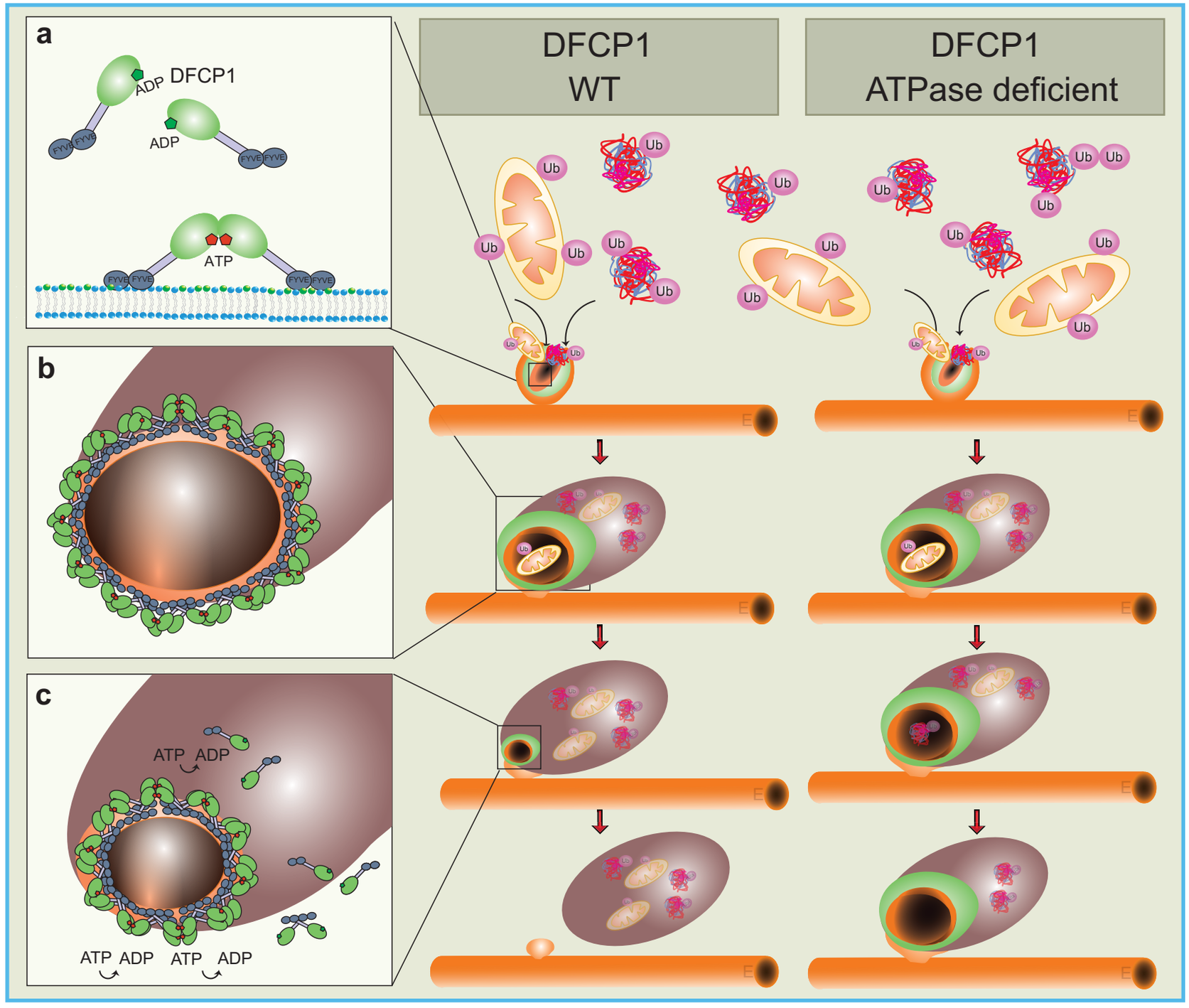
a
ADP DFCP1
FYVE FYVE
ADP
FYVE FYVE
ATP
FYVE FYVE FYVE FYVE
b
c
ATP ADP
ATP ADP ATP ADP
DFCP1
WT
DFCP1
ATPase deficient
Ub
E

Extended Data Fig.9: Model of how DFCP1 acts at the omegasome during selective autophagy.

(a) Omegasome initiation: Upon induction of selective autophagy, PtdIns3P is generated at specialized subregions of the ER, at omegasomes. The FYVE domains of DFCP1 bind to these PtdIns3P pools and DFCP1 is assembled at the omegasome. ATP-binding of DFCP1 leads to its multimerization and could potentially generate a platform to bind ubiquitinated cargo. The phagophore is assembled within the omegasome cradle.

(b) Omegasome maturation: the omegasome ring expands, accumulating DFCP1 dimers which form larger assemblies. This accumulation is likely driven by PtdIns3P at the omegasome. Nucleotide binding and multimerization stabilize DFCP1 at the omegasome.

(c) Omegasome constriction: Repeated cycles of ATP loading and hydrolysis drive the constriction of the omegasome ring. Constriction can either be achieved by transient disassembly of DFCP1 and the loss of some subunits, or alternatively, DFCP1 molecules can repeatedly engage neighboring molecules and constrict the membrane by a ratchet-like mechanism. DFCP1 mutants – either nucleotide binding defective of hydrolysis defective – cannot perform this repeated cycling. This leads to an inefficient constriction of the omegasome ring, the accumulation of omegasomes, and an inefficient degradation of selective cargo.